Water Adsorption in Carbon-Slit Nanopores

Alberto Striolo,† Ariel A. Chialvo,‡ Peter T. Cummings,‡,§ and Keith E. Gubbins*,†

Department of Chemical Engineering, North Carolina State University, 113 Riddick Labs, Raleigh, North Carolina 27695-7905, Chemical Sciences Division, Oak Ridge National Laboratory, Oak Ridge, Tennessee 37831-6110, and Department of Chemical Engineering, Vanderbilt University, Nashville, Tennessee 37235-1604

Received April 30, 2003. In Final Form: July 16, 2003

With the use of the grand canonical Monte Carlo simulation, water adsorption isotherms were determined for SPC/E water in slit-shaped graphitic nanopores at 298 K. The pore widths considered were 0.6, 0.625, 0.7, 0.8, 1.0, 1.6, and 2.0 nm. The resulting adsorption isotherms indicated negligible adsorption at low pressures, pore-filling by a capillary-condensation-like mechanism, and adsorption/desorption hysteresis loops. For pore widths equal to or larger than 0.7 nm, the relative pressure at which pore filling occurs and the size of the hysteresis loop decrease with decreasing pore width. For 0.6-nm pores, pore filling occurs at pressures approaching saturation. Upon decreasing the pore width from 2.0 to 0.7 nm, the zero-coverage isosteric heat of adsorption increases from 6 to 14 kJ/mol. The limit at high coverage converges to the enthalpy of condensation for SPC/E water as the pore width increases. From the simulated adsorbed-water densities and distributions across the pores and the use of a mean-field approximation, the solvation force was computed between two flat hydrophobic walls. The force profile oscillates as a function of the wall-to-wall separation. Our results show that attractive peaks of the force correspond to wall-to-wall separations at which confined water molecules cannot establish a finite number of layers, while repulsive peaks correspond to separations at which confined water molecules form well-defined layers of molecules, often stabilized by intralayer hydrogen bonds.

Introduction

Porous carbon materials are used for separation, purification, and catalysis purposes.[1−3] While the adsorption and phase behavior of nonpolar fluids in carbon pores has been studied extensively,[4,5] our understanding regarding adsorption of water in carbonaceous materials is still rudimentary. Nevertheless, the structure and the thermodynamic properties of water confined in hydrophobic regions are of importance in many scientific disciplines such as chemistry, geology, nanotechnology, and biology. Water adsorption in hydrophobic materials is typically characterized by negligible adsorption at low relative pressures, sudden and complete pore filling by a capillary-condensation mechanism, and large adsorption/desorption hysteresis loops.[6,7]

Experimental observations alone do not allow us to understand water adsorption because of the small pore size that characterizes carbons, their peculiar morphologies, and the frequent appearance of long-lived metastable states for the adsorbed water. It is generally believed that the combination of weak carbon−water dispersive attractions and strong water−water associative interactions is responsible for the complex behavior of water confined in graphitic pores. In this scenario, molecular simulation becomes a powerful tool for investigating phenomena from a molecular point of view and, thus, to test this hypothesis.[8]

Previous simulations for water adsorption in carbons involved mainly slit pores 2-nm wide.[9−11] While this simple representation of a pore is adequate to describe graphitic matrixes, it might be inappropriate to represent industrial adsorbents. Industrial materials are in fact characterized by pore size polydispersity, pore interconnectivity, and heterogeneous chemical composition.[12,13] However, the slit geometry allows us to modulate carbon−water interactions by varying the pore width. In fact, pore−water interactions become more attractive by reducing the pore width because of the cooperative effect between the approaching attractive walls. However, by reducing the pore width, the water molecules become confined in a two-dimensional region, and the characteristic tetrahedral hydrogen-bonded network becomes distorted.

The aim of this work is to understand whether the peculiarities observed in experimental adsorption isotherms for water may be ascribed to weak carbon−water interactions relative to strong water−water ones. To accomplish our goal, we have investigated the effect of the pore width upon the characteristics of adsorption isotherms for water in carbon-slit pores. Chemical heterogeneity in the porous material and pore interconnectivity are not accounted for.

The pore widths considered were 0.6, 0.625, 0.7, 0.8, 1.0, 1.6, and 2.0 nm. The pore width H is the minimum distance between the centers of the carbon atoms belonging to the graphene layers on the surface of the

* Author to whom correspondence should be addressed. E-mail: keg@ncsu.edu.
† North Carolina State University.
‡ Oak Ridge National Laboratory.
§ Vanderbilt University.

(1) Rudisill, E. N.; Hacskaylo, J. J.; Le Van, M. D. *Ind. Eng. Chem. Res.* **1992**, *31*, 1122.
(2) Sircar, S.; Golden, T. C.; Rao, M. B. *Carbon* **1996**, *34*, 1.
(3) Seaton, N. A.; Friedman, S. P.; MacElroy, J. M. D.; Murphy, B. J. *Langmuir* **1997**, *13*, 1199.
(4) Jiang, S.; Rhykerd, C. L.; Gubbins, K. E. *Mol. Phys.* **1993**, *79*, 373.
(5) Cracknell, R. F.; Nicholson, D.; Quirke, N. *Mol. Phys.* **1993**, *80*, 885.
(6) Gregg, S. J.; Sing, K. S. W. *Adsorption, Surface Area and Porosity*; Academic Press: London, 1982.
(7) Brennan, J. K.; Bandosz, T.; Thomson, K. T.; Gubbins, K. E. *Colloids Surf., A* **2001**, *187−188*, 539.
(8) Nicholson, D. *J. Chem. Soc., Faraday Trans.* **1996**, *92*, 1.
(9) Ulberg, D. E.; Gubbins, K. E. *Mol. Phys.* **1995**, *84*, 1139.
(10) Müller, E. A.; Gubbins, K. E. *Carbon* **1998**, *36*, 1433.
(11) McCallum, C. L.; Bandosz, T. J.; McGrother, S. C.; Müller, E. A.; Gubbins, K. E. *Langmuir* **1999**, *15*, 533.
(12) Segarra, E. I.; Glandt, E. D. *Chem. Eng. Sci.* **1994**, *49*, 2953.
(13) Thomson, K. T.; Gubbins, K. E. *Langmuir* **2000**, *16*, 5761.

10.1021/la0347354 CCC: $25.00
Published on Web 09/06/2003

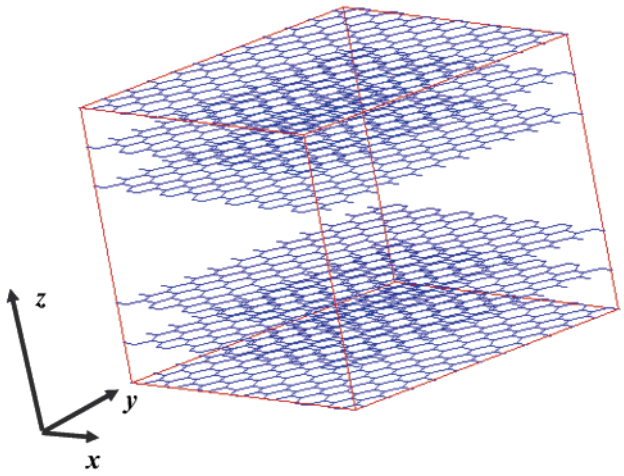

Figure 1. Schematic representation for the simulated carbon-slit pores. Three graphene layers are considered both above and below the pore.

opposing pore walls. Three layers of graphite are considered on either side of the pore. A schematic representation of a pore used in our simulations and the *x*, *y*, and *z* axes are shown in Figure 1. For clarity, the carbon atoms are not represented explicitly. However, it should be noted that the Lennard-Jones diameter of a carbon atom is 0.34 nm while the center-to-center distance between neighboring atoms in a graphite layer is 0.142 nm. Thus, the graphite surface is relatively smooth on the length scale of a water molecule. The layers of carbon atoms considered are commensurate. This representation slightly reduces the smoothness of the surface. Several experimental observations[7,14,15] find a sound explanation within the simple molecular model employed here. In particular, our results show that pore filling happens by a capillary-condensation-like mechanism for each pore width considered. For pores wider than 0.7 nm, the relative pressure at which pore filling occurs and the size of the adsorption/desorption hysteresis loop decrease with decreasing pore width. A molecular-sieve effect is found when pores are narrower than 0.7 nm.

From the adsorbed-water densities and their distribution across the pores as a function of the pore width, the solvation force between approaching hydrophobic walls was calculated at thermodynamic conditions close to saturated bulk liquid water. In agreement with others,[9,16−18] our results for the solvation pressure show an oscillatory behavior as a function of the wall-to-wall distance and can be related to the structure of the confined water. Attractive peaks correspond to wall-to-wall separations where confined water molecules are not allowed to establish a finite number of layers, while repulsive peaks correspond to separations where a finite number of well-established layers are formed and often stabilized by intralayer hydrogen bonds.

Simulation Methodology

(a) Water Model. Most of the peculiarities of water are due to its capability to form orientation-specific hydrogen bonds.[19] Simulation studies of confined water are not abundant in the literature. Among several water models available (for a detailed review see ref 20), we chose the SPC/E[21] because it satisfactorily reproduces the structure of bulk liquid water from room to supercritical conditions[22] and because water−water interactions are accounted for with a spherical cutoff so that no long-range corrections for electrostatic interactions are required.

In the SPC/E model, water is represented as a sphere with the oxygen atom located in its center. The center of the sphere is also the site responsible for dispersive water−water interactions, described by a Lennard-Jones potential. The sites representative of the hydrogen atoms are located at a distance of 0.1 nm from the oxygen site; the hydrogen−oxygen−hydrogen angle is 109.5°. Partial charges are placed on the oxygen and on the hydrogen sites so as to capture the electrostatic interactions. The charge on the oxygen site equals −0.8476e, while each of those located at the hydrogen sites equals +0.4238e. The water−water interaction potential is given by

$$u_{OO} = \sum_{i=1}^{3}\sum_{j=1}^{3} \frac{q_i q_j}{4\pi\epsilon_0 r_{ij}} + 4\epsilon_{OO}\left[\left(\frac{\sigma_{OO}}{r_{OO}}\right)^{12} - \left(\frac{\sigma_{OO}}{r_{OO}}\right)^{6}\right] \quad (1)$$

In eq 1, ϵ_0 is the permittivity of the vacuum (8.854×10^{-12} C^2 J^{-1} m^{-1}), q_i is the partial charge localized on each charged site, r_{ij} is the distance between sites in different molecules, r_{OO} is the distance between oxygen sites in the pair of water molecules, and ϵ_{OO} and σ_{OO} are the corresponding Lennard-Jones energy and size interaction parameters.

(b) Graphite Pore Model. The carbon atom in the graphite matrix is represented as a Lennard-Jones sphere, and its interaction with water u_{OC} is given by

$$u_{OC}(r_{OC}) = 4\epsilon_{OC}\left[\left(\frac{\sigma_{OC}}{r_{OC}}\right)^{12} - \left(\frac{\sigma_{OC}}{r_{OC}}\right)^{6}\right] \quad (2)$$

In eq 2, r_{OC} is the distance between the oxygen in the water molecule and the carbon atom. The unlike Lennard-Jones interaction parameters σ_{OC} and ϵ_{OC} are described by the Lorentz−Berthelot combining rules:

$$\sigma_{OC} = \frac{\sigma_{OO} + \sigma_{CC}}{2} \quad (3)$$

$$\epsilon_{OC} = \sqrt{\epsilon_{OO}\epsilon_{CC}}$$

When the graphitic pore is described as a structureless infinite pore, pore−water interactions can be represented by the (10,4,3) potential that depends only on the axial distance *z* between the water molecule and the wall:[23]

$$u_{OC}(z) = 2\pi\rho_c\epsilon_{OC}\sigma_{OC}{}^2\Delta\left[\frac{2}{5}\left(\frac{\sigma_{OC}}{z}\right)^{10} - \left(\frac{\sigma_{OC}}{z}\right)^{4} - \left(\frac{\sigma_{OC}{}^4}{3\Delta(z + 0.61\Delta)^3}\right)\right] \quad (4)$$

(14) Iiyama, T.; Mishikawa, K.; Otowa, T.; Kaneko, K. *J. Phys. Chem.* **1995**, *99*, 10075.
(15) Hanzawa, Y.; Kaneko, K. *Langmuir* **1997**, *13*, 5802.
(16) Lüzar, A.; Bratko, D.; Blum, L. *J. Chem. Phys.* **1987**, *86*, 2955.
(17) Bratko, D.; Curtis, R. A.; Blanch, H. W.; Prausnitz, J. M. *J. Chem. Phys.* **2001**, *115*, 3873.
(18) Koga, K. *J. Chem. Phys.* **2002**, *116*, 10882.
(19) Eisenberg, D.; Kauzmann, W. *The Structure and Properties of Water*; Oxford University Press: New York, 1969.
(20) Chialvo, A. A.; Cummings, P. T. Molecular-Based Modeling of Water and Aqueous Solutions at Supercritical Conditions. *Adv. Chem. Phys.* **1999**, *109*, 115.
(21) Berendsen, H. J. C.; Grigera, J. R.; Straatsma, T. P. *J. Phys. Chem.* **1987**, *91*, 6269.
(22) Chialvo, A. A.; Yezdimez, E.; Driesner, T.; Cummings, P. T.; Simonson, J. M. *Chem. Phys.* **2000**, *258*, 109.
(23) Steele, W. A. *The Interaction of Gases with Solid Surfaces*; Pergamon Press: Oxford, 1974.

Table 1. Lennard-Jones Parameters for Water−Water and Carbon−Carbon Dispersive Interactions[a]

	σ (nm)	ϵ/k
water−water	0.3166	78.23
carbon−carbon	0.340	28.00

[a] ϵ is the minimum depth of the interaction potential, and σ is the center-to-center distance when the potential passes through 0. k is the Boltzmann constant.

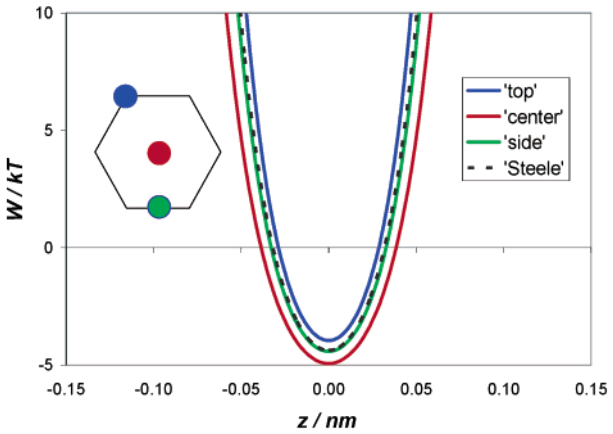

Figure 2. Pore−water interaction potential across pores 0.6-nm wide as a function of the position of the water molecule with respect to the graphite layer. The inset shows the three positions considered for a water molecule. The three positions are defined as the *center* of the hexagon, on *top* of a carbon atom, and on the *side* of the hexagon. The pore−water interaction potential obtained with the Steele (10,4,3) approximation (eq 4) is also shown for comparison.

In eq 4, ρ_c is the density of carbon atoms and Δ is the distance between sheets of carbons, where these parameters for graphite are $\rho_c = 114$ nm^{-3} and $\Delta = 0.335$ nm.

The potential energy of a water molecule within the pore is given by the sum of its interactions with each wall plus those with other water molecules in the pore. Pairwise additivity is considered for all interactions. The Lennard-Jones parameters used are given in Table 1.

The pore−water Lennard-Jones potential when a water molecule is within a 0.6-nm-wide pore is shown in Figure 2 as a function of the position across the pore. Different $x-y$ sites are considered for the confined water molecule with respect to the graphite layer. The positions considered are at the *center* of the carbon-atom hexagon, on *top* of a carbon atom, and at the *side* of the carbon-atom hexagon. The pore−water potential is obtained by explicitly considering each carbon−water pair interaction. The most favorable position for an adsorbed water molecule is the *center* position, while the least favorable position is the *top* site. In Figure 2 is also shown the Steele (10,4,3) potential (eq 4), which represents an average of the pore−water interaction potentials obtained at various $x-y$ positions. Adsorption isotherms for water in 1.6-nm-wide pores obtained using the Steele potential (eq 4) and with the sum of each carbon−water pair interaction did not show appreciable differences. Thus, the Steele potential was considered adequate to compute adsorption isotherms in pores wider than 1.6 nm. For pores narrower than 1.6 nm, the pore−water interactions were computed by accounting for all the water−carbon pair interactions within the pore. It should be noted that by considering commensurate carbon layers the difference between the pore−water interaction potentials as a function of the $x-y$ positions of the water molecules within the pores is increased. For computational efficiency, a grid was built with 0.015-nm spacing, and linear interpolation was used between the points in the grid.

(c) Simulation Scheme. The grand canonical Monte Carlo (GCMC) method[24−26] was used to simulate water adsorption. In this ensemble, the volume, temperature, and adsorbate chemical potential are fixed. The number of adsorbate molecules can vary, as well as the location and the orientation of each adsorbed molecule within the pore. Trial moves considered were the translation, rotation, insertion, and deletion of water molecules. The moves were randomly chosen with equal probability to ensure microscopic detailed balance. The maximum translation vector was automatically adjusted to obtain an acceptance ratio of about 0.35. The rotations were obtained with the quaternions method.[25] No limitation was imposed on the maximum rotation angle. The acceptance ratio for rotation trial moves was at least 0.20.

To allow simulation of a periodic box constituted by arrays of hexagons representing the graphite plate, x and y simulation-box sizes were 2.95 and 2.98 nm, respectively. Periodic boundary conditions were applied in the x and y directions. Some of the simulations presented here were performed in larger pores (4.69 × 4.43 nm in the x and y directions), and no significant differences in the results were observed.

For the adsorption path, mimicking experimental procedures, the pores were first considered empty. Simulation runs were performed at increasing chemical potentials. The resulting simulation configurations were then used as the starting point for the subsequent simulation at higher chemical potentials. Desorption cycles were initiated with a typical configuration of a filled pore. The chemical potential was then slowly reduced until the pores were emptied from the previously confined water.

Equilibration runs as long as 200 million (2×10^8) trial moves were required. The production phase involved at least 1.5 billion (1.5×10^9) trial moves. Longer runs (up to 3 billion trial moves) were required when the system was close to capillary condensation. In the wider pores considered, up to approximately 500 water molecules may be adsorbed in correspondence to pore filling. During a typical production run, accepted deletion/insertion moves guarantee that all adsorbed water molecules are substituted at least 10 000 times; thus, the implementation of insertion/deletion biasing techniques was not necessary.

To obtain the reduced pressure of the bulk phase in equilibrium with the adsorbate at various chemical potentials, a virial equation of state that employs a known saturation point was used.[27] The chemical potential and the density for the bulk saturated vapor are required at the considered temperature. Separate simulation runs were conducted to obtain these values.

Because of excluded-volume effects, the effective pore width available to adsorbed water molecules, which is less than the width H, cannot be defined unambiguously. Thus, the adsorbed-water density is reported here in terms of the surface coverage, ξ, defined as the number of adsorbed water molecules per square nanometer of porous surface.

Among other quantities of interest, we have computed the isosteric heat of adsorption, the oxygen- and hydrogen-

(24) Nicholson, D.; Parsonage, N. G. *Computer Simulation and the Statistical Mechanics of Adsorption*; Academic Press: London, 1982.
(25) Allen, M. P.; Tildesley, D. J. *Computer Simulation of Liquids*; Clarendon Press: Oxford, 1987.
(26) Frenkel, D.; Smit, B. *Understanding Molecular Simulation*, 2nd ed.; Academic Press: London, 2002.
(27) Müller, E. A.; Rull, L. F.; Vega, L. F.; Gubbins, K. E. *J. Phys. Chem.* **1996**, *100*, 1189.

atom density distributions across the pore, and the axial order parameter S along the z direction. The isosteric heat of adsorption was computed according to[24]

$$q_{st} \cong -\frac{\langle NU\rangle - \langle N\rangle\langle U\rangle}{\langle N^2\rangle - \langle N\rangle\langle N\rangle} + kT \qquad (5)$$

In eq 5, N is the total number of adsorbed water molecules, U is the system configurational internal energy, k is the Boltzmann constant, and the angular brackets denote ensemble averages. While the average number of adsorbed molecules was generally stable after 100 million Monte Carlo moves, equilibration for q_{st} required longer production runs.

The oxygen- and hydrogen-atom density profiles across the pore were computed as

$$\rho_i^*(z) = \frac{\langle N_i(z, z + dz)\rangle}{\langle N_i\rangle XY\, dz} \qquad (6)$$

In eq 6, the subscript i is for either oxygen or hydrogen, X and Y are the planar dimensions of the simulation box, dz is the width of the pore slab considered to compute the local density, and N_i is the number of adsorbed atoms i.

The order parameter S was computed as

$$S = \frac{3\langle\cos^2\vartheta\rangle - 1}{2} \qquad (7)$$

where ϑ is the angle between the dipole moment of the water molecule and the z direction of the pore. When the dipoles of the water molecules are perpendicular to the pore walls, $S = 1$; when the dipoles are parallel to the pore walls, $S = -0.5$.

Simulation Results and Discussion

(a) Adsorption Isotherms. Water adsorption isotherms simulated in 0.6- and 1.6-nm-wide carbon-slit pores are shown in Figure 3. Results are obtained by computing the pore−water potential as the sum of each carbon−water interaction and by the Steele (10,4,3) potential. For H = 1.6 nm (Figure 3a), the difference between the simulated adsorption isotherms is negligible; in particular, the adsorption/desorption loop and the amounts adsorbed after pore filling are slightly larger when the Steele (10,4,3) potential is considered. When H = 1.6 nm, results for the isosteric heat of adsorption and for the structure of confined water are also equivalent when pore−water interactions are accounted for by the Steele (10,4,3) potential or by the sum of each carbon−water pair interaction. The small differences observed in the two cases are probably due to the fact that the Steele (10,4,3) potential accounts for an infinite number of graphite layers on each side of the pore, while our pore representations (see Figure 1) account only for three graphite layers, and, thus, it is less attractive.

However, when the pore width is 0.6 nm (Figure 3b), the difference between simulated adsorption isotherms is relevant. In particular, when pore−water interactions are represented by the Steele (10,4,3) potential pore filling occurs at lower relative pressure and the hysteresis loop is slightly narrower. When the pore width is 0.6 nm, the difference between the infinite number of graphene layers accounted for in the Steele (10,4,3) potential and the three layers in the explicit potential with every carbon−water pair interaction accounted for is not sufficient to explain the differences observed in Figure 3b (see Figure 2 for pore−water potential energies in the two approximations).

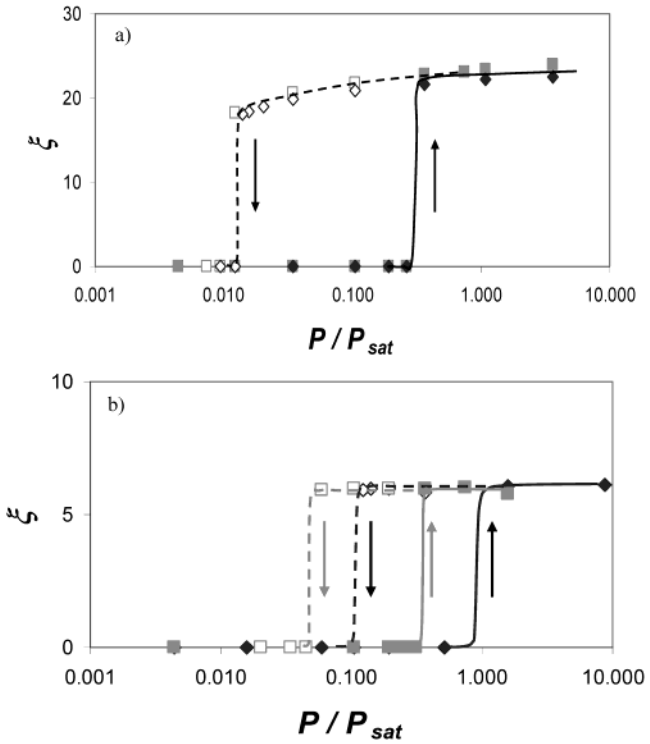

Figure 3. Coverage of the porous surface, ξ (number of adsorbed molecules per square nanometer of porous surface), as a function of the relative pressure for water adsorbed in carbon-slit pores at 298 K. Part a is for H = 1.6 nm. Part b is for H = 0.6 nm. Full symbols are for adsorption; open symbols are for desorption. Gray squares are obtained by using the Steele potential to account for pore−water interactions, while black diamonds are for results obtained by considering each carbon−water interaction potential. Lines are guides to the eye. Symbols are larger than the simulation uncertainty. Arrows indicate the sequence of results obtained at increasing or decreasing pressure (adsorption and desorption, respectively).

When a strongly associating fluid such as water is confined in narrow pores, the roughness of the surface may promote or frustrate the formation of energetically favorable networks of hydrogen-bonded adsorbed molecules. Therefore, when nanopores are considered it is preferable to consider an atomistic description of the adsorbent material to properly describe the structure and the thermodynamic properties of the confined fluid.

Water adsorption isotherms computed at 298 K are shown in Figure 4. Simulated adsorption isotherms are of type V.[6,28] Simulation results qualitatively agree with available experimental observations:[7,11,14,15] at a low relative pressure, water is adsorbed only in narrow pores (H less than about 1.5 nm), while higher relative pressures (above 0.80) are required for pore filling to occur in wider pores.

Pore filling occurs at pressures close to saturation for 2.0-nm-wide pores. By reducing the pore width from 2.0 to 0.7 nm, the relative pressure at which pore filling occurs decreases significantly. The adsorption isotherm for water in 0.6-nm-wide pores is characterized by capillary evaporation. At these conditions, the pore fills only at pressures close to saturation. These findings can be explained by observing the pore−water potential as a function of the pore width (Figure 5a). By reducing the pore width from 2.0 to 0.7 nm, the pore−water potential becomes more attractive, but adsorbed molecules are constrained in a

(28) Rouquerol, F.; Rouquerol, J.; Sing, K. *Adsorption by Powders and Porous Solids*; Academic Press: London, 1999.

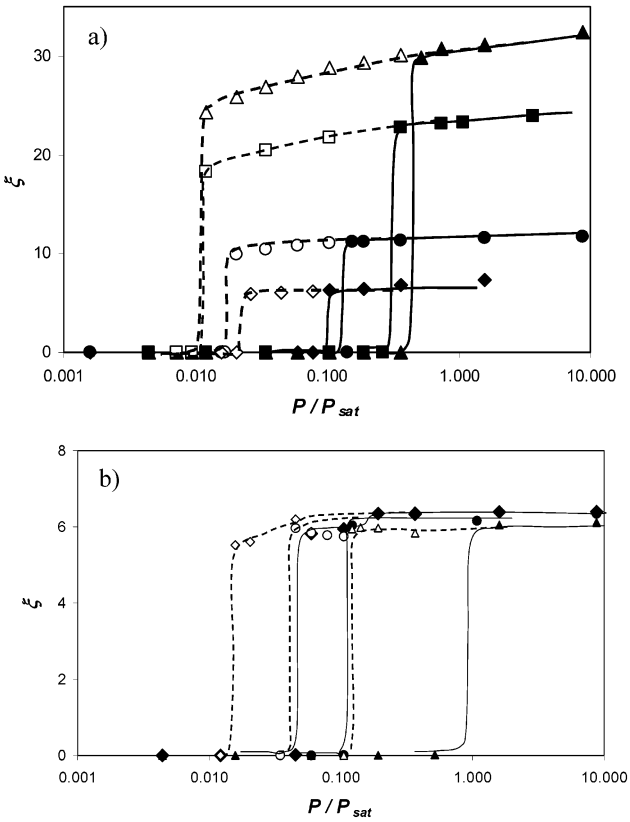

Figure 4. Coverage of the porous surface, ξ, as a function of the relative pressure for water adsorbed in carbon-slit pores at 298 K. Part a shows the results obtained in pores of width 0.8 (diamonds), 1.0 (circles), 1.6 (squares), and 2.0 (triangles) nm. Part b shows the results obtained in pores of width 0.7 (diamonds), 0.625 (circles), and 0.6 (triangles) nm. Full symbols represent results for adsorption, while open symbols are for the desorption loops. Lines are guides to the eye. Symbols are larger than the simulation uncertainty. Pore−water interactions are computed using the Steele potential when $H = 2.0$ nm and by considering each carbon−water pair interaction in all other cases.

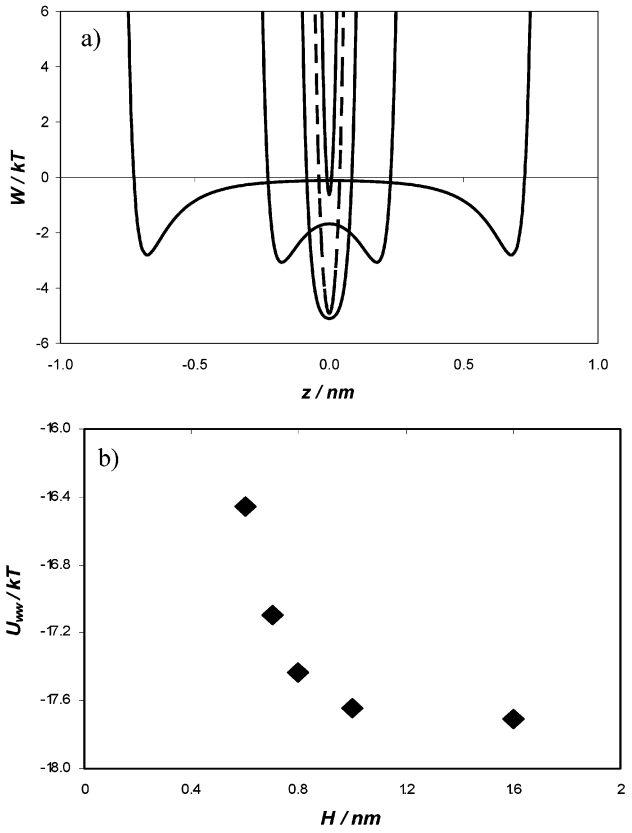

Figure 5. Pore−water interaction potential, W, across the pore (part a) and water−water internal energy, U_{ww} (part b), as a function of the pore width. In part a, the pore widths considered are 0.55, 0.6, 0.7, 1.0, and 2.0 nm. The broken line is for $H =$ 0.6 nm. The potentials are computed assuming the central position of an adsorbed water molecule (see Figure 2 for details). In part b, U_{ww}, expressed on a "per-adsorbed-water-molecule" basis, was computed at conditions of saturated bulk liquid SPC/E water at 298 K. The pore widths considered are 0.6, 0.7, 0.8, 1.0, and 1.6 nm.

narrower region. When water molecules are confined in 0.6-nm pores, the tetrahedral hydrogen-bonded network, typical of liquid water, is frustrated and higher pressures are required to fill the pore with liquid water. At H=0.55 nm, the pore−water interaction becomes repulsive because of excluded-volume effects. The fluid−fluid configurational internal energy for confined water as a function of the pore width at conditions corresponding to saturated bulk liquid SPC/E water is shown in Figure 5b. Results are expressed in a "per-adsorbed-water-molecule" basis. Our results suggest that the water−water configurational internal energy, representative of hydrogen bonds among adsorbed molecules, increases when the pore width is decreased from 1.6 to 0.6 nm. These results provide further evidence that the hydrogen-bonded network between adsorbed water molecules is frustrated when the pore width is reduced to 0.6 nm.

Adsorption/desorption hysteresis loops are also shown in Figure 4; these are surprisingly wide, even though these results are in qualitative agreement with available experimental observations.[15] The size of the hysteresis loops decreases with decreasing pore width. Also, the shape of the hysteresis loops changes slightly with decreasing pore width. While the general shape is rectangular, the upper part of the hysteresis loop, along the desorption path, decreases with decreasing pressure for larger pores but seems to remain constant for narrower pores.

The density−temperature points within the hysteresis loops may be representative of metastable states in which the system is trapped in local minima of the free-energy landscape.[29] It is not clear why hysteresis appears and why it is correlated to capillary-condensation phenomena. One possible explanation relies on the different interfacial surface areas during the adsorption and desorption phases. When a liquid phase grows within a vapor phase, the interfacial area is less than that when a vapor phase grows within a liquid phase. As a result of this difference in interfacial surface areas, hysteresis loops appear in simulated and experimental adsorption isotherms.[6] In Figure 6, some intermediate configurational snapshots collected during desorption of water from a 0.6-nm-wide pore are shown.

The sequence of snapshots shows that, during desorption from a filled pore, first the quasi-ordered structure of the confined fluid is lost. Then, several low-density regions ("bubbles") appear within the pore. Finally, density fluctuations cause these bubbles to coalesce and grow, until the pore empties. Results for the adsorption mechanism, not shown for brevity, show that adsorption happens by growth of clusters of water molecules. The number of clusters of water molecules during pore filling is lower than the number of bubbles during pore emptying;

(29) Gelb, L. D.; Gubbins, K. E.; Radhakrishnan, R.; Sliwinska-Bartkowiak, M. *Rep. Prog. Phys.* **1999**, *62*, 1573.

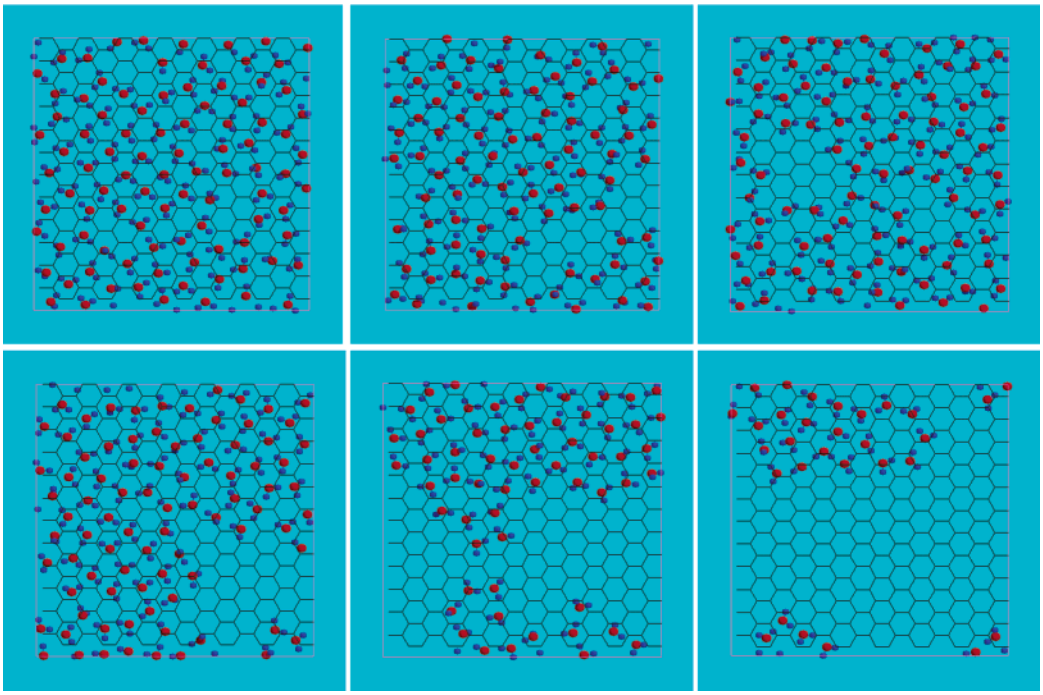

Figure 6. Intermediate configurational snapshots collected during the desorption of water from pores 0.6-nm wide at 298 K. The starting configuration was that of a pore filled with water. Snapshots, presented in sequence from left to right, top to bottom, show the desorption of SPC/E water computed at a relative pressure equal to 0.1, which was maintained constant until the pore empties. The red dots represent oxygen atoms; the blue ones represent hydrogen atoms. The graphite plane is represented with black lines.

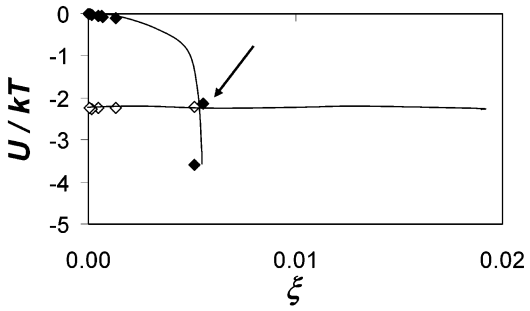

Figure 7. Pore−water (open symbols) and water−water (full symbols) configurational internal energy as a function of the water coverage for water adsorbed in pores 1.0-nm wide at 298 K. The energies are expressed in a "per-adsorbed-water-molecule" basis. The results reported are for the adsorption process. The arrow approximately indicates the conditions at which pore filling occurs. Lines are guides to the eye.

hence, the interfacial surface area is larger during desorption than during adsorption.

The mechanism of pore filling via capillary condensation is related to the relative strength of adsorbent−adsorbate and of adsorbate−adsorbate interactions. The pore−water and the water−water configurational internal energies are shown in Figure 7 as a function of the surface coverage for water adsorbed in 1.0-nm-wide carbon-slit pores. Results are expressed in a "per-adsorbed-water-molecule" basis. Similar results are obtained for the other pores studied here. Figure 7 indicates that, as expected for pore filling by a capillary-condensation-like mechanism, pore filling occurs when water−water interactions become dominant over pore−water interactions.

The isosteric heat of adsorption is shown in Figure 8 as a function of coverage for water adsorbed in the pores considered here. Because of increased pore−water attraction, the limit of 0 coverage for q_{st} (Figure 8a) increases with decreasing pore width. The value of q_{st} computed for water in 0.7-nm-wide pores is lower than that obtained by Bagreev et al.[30] on a similar system. However, the Lennard-Jones attraction parameter used by Bagreev et al. is larger than that used here. Experimental results show that q_{st} at large coverages converges to the enthalpy of condensation for water (43.6 kJ/mol).[7] Our results for q_{st} at high coverages, as is shown in Figure 8b, converge to the enthalpy of condensation of SPC/E water[31] as the pore width increases.

(b) Structure of Confined Water. The oxygen- and hydrogen-atom density profiles across the 2.0-nm-wide pores are shown in Figure 9 for increasing pressures before and after pore filling. Before pore filling, because of attractive wall−water interactions, adsorbed water molecules preferentially occupy the regions close to the adsorbing walls (Figure 9a). The surface coverage at these conditions is lower than 0.005 molecules/nm^2; thus, there is no formation of an adsorbed monolayer. At pore filling, the adsorbed water molecules fill the pore completely (Figure 9b). In agreement with others,[9,17,32,33] our results show the formation of one or two fluid layers in contact with each adsorbing wall, while at further distances from the confining walls the density becomes uniform. Only at much higher pressures does the density profile across the pore indicate the formation of six distinct layers of adsorbed water (Figure 9c).

The order parameter S across pores of width 2.0 nm is displayed in Figure 10 for adsorbed water before and soon after pore filling. In agreement with simulation results for TIP4P water in carbon-slit pores,[9] Figure 10a indicates that before pore filling no specific ordering of the adsorbed molecules is observed. After pore filling (Figure 10b), water

(30) Bagreev, A.; Bashkova, S.; Bandosz, T. J. *Langmuir* **2002**, *18*, 8553.
(31) Glättli, A.; Daura, X.; van Gunsteren, W. F. *J. Chem. Phys.* **2002**, *116*, 9811.
(32) Lee, S. H.; Rasaiah, J. C.; Hubbard, J. B. *J. Chem. Phys.* **1987**, *86*, 2383.
(33) Jönsson, B. *Chem. Phys. Lett.* **1981**, *82*, 520.

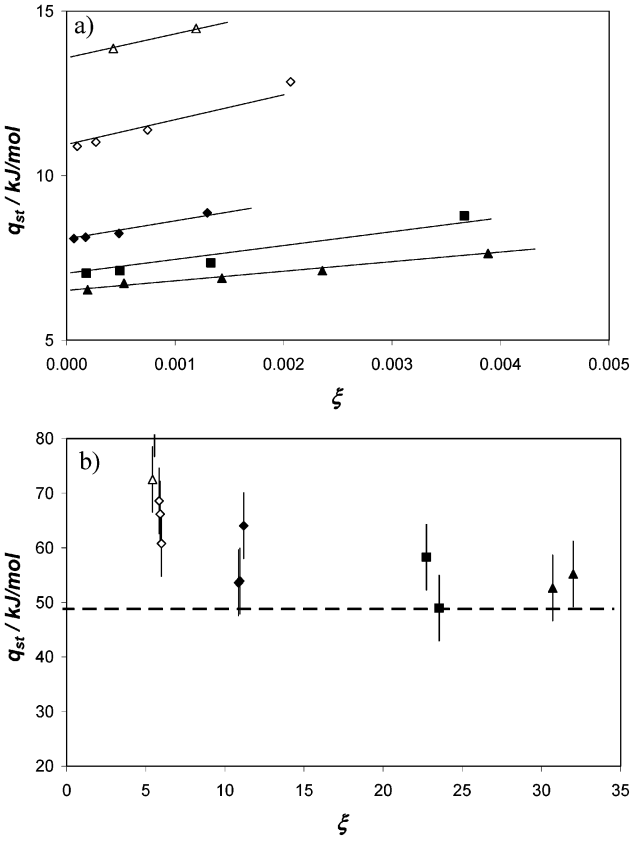

Figure 8. Isosteric heat of adsorption, q_{st}, as a function of the surface coverage, ξ, for water adsorption in the pores considered here. Parts a and b are for the limits at low and high coverage for q_{st} (lines are guides to the eye). In part b, the broken line indicates the enthalpy of liquefaction for SPC/E water at 298 K (48.8 kJ/mol).[31] Closed triangles are for $H = 2.0$ nm, closed squares are for $H = 1.6$ nm, closed diamonds are for $H = 1.0$ nm, open diamonds are for $H = 0.8$ nm, and open triangles are for $H = 0.7$ nm. The uncertainty is smaller than the symbols in part a. Estimated error bars are shown in part b.

molecules in the first adsorbed monolayer tend to orient their dipole moments parallel to the hydrophobic surface. Inner water molecules do not show a clear orientation with respect to the pore surfaces.

Oxygen- and hydrogen-atom density profiles across the 1.0-nm-wide pore after pore filling are shown in Figure 11a. Results for the oxygen-atom density profile suggest the formation of two adsorbed monolayers in contact with the hydrophobic surfaces. These two layers are bound by intralayer hydrogen bonds, as can be seen by the relative maximum in the hydrogen-atom density profile in the central region of the pore. The order parameter S across pores 1.0-nm wide after pore filling is shown in Figure 11b. As was observed for water confined in pores 2.0 nm wide (Figure 10b), the adsorbed water molecules orient their dipole moments parallel to the pore surface; this orientation helps to establish a hydrogen-bonded network between confined molecules.

Typical snapshots for water adsorbed in pores 1.0-nm wide after pore filling are shown in Figure 12. From the top view (Figure 12a), it is clear that the confined water behaves as a fluid. Results for oxygen−oxygen, oxygen−hydrogen, and hydrogen−hydrogen radial distribution functions, not shown for brevity, corroborate this observation. The lateral view (Figure 12b) supports the image of a two-layered hydrogen-bonded structure for the confined water (see also Figure 11). While this two-layered structure resembles that found for TIP4P water confined

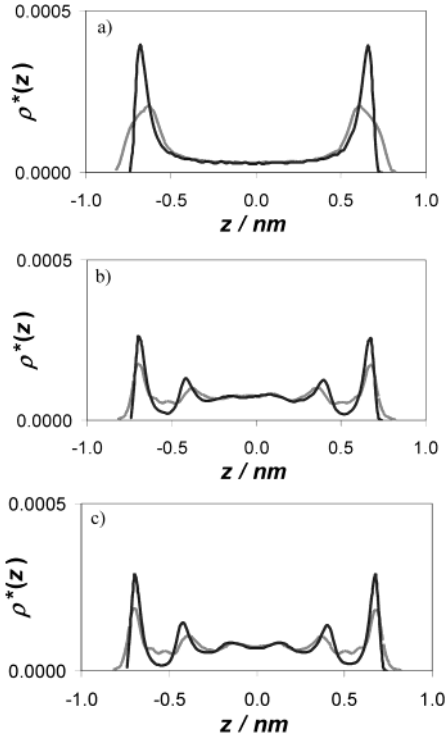

Figure 9. Oxygen-atom (black lines) and hydrogen-atom (grey lines) density profiles across pores 2.0-nm wide at increasing chemical potential before (part a, $P/P_0 = 0.04$) and after (part b, $P/P_0 = 1.60$; part c, $P/P_0 = 10$) pore filling. Pore−water interactions are accounted for using the Steele potential.

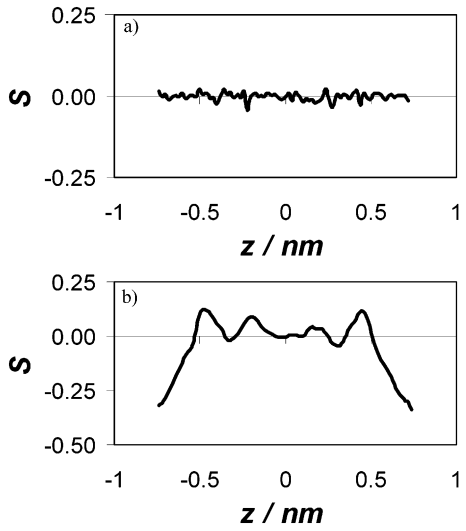

Figure 10. Order parameter S across pores 2.0-nm wide at increasing relative pressure. Conditions before (part a, $P/P_0 = 0.04$) and after (part b, $P/P_0 = 1.6$) pore filling are shown. Pore−water interactions are accounted for using the Steele potential.

in narrow hydrophobic walls at 270 K and 0.1 MPa by Koga et al.,[34] there are also significant differences. In particular, the structure presented here is that of a fluid rather than that of an amorphous solid, and the two layers are not superimposed on each other. It is possible that subtle differences in the models employed for water and for the pore−water potential are the cause of the discrepancy between our results and those presented by Koga et al. and that four- or five-site water models are required to properly capture the structure of confined solid structures.

(34) Koga, K.; Tanaka, H.; Zeng, X. C. *Nature* **2001**, *412*, 6849.

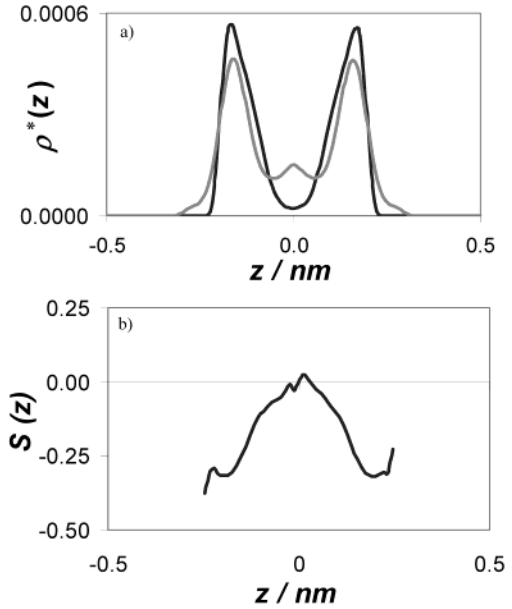

Figure 11. Structure of water confined in pores 1.0-nm wide at relative pressures equal to 0.8. In part a, the oxygen-atom (black line) and hydrogen-atom (grey line) density profiles across the pore are shown. The order parameter S across the pore is shown in part b at the same conditions considered in part a. Each carbon−water pair interaction is accounted for to obtain the pore−water potential.

(c) Solvation Pressure. The solvation pressure can be related to the density profile of an adsorbate across a slit pore:[35]

$$P_{\mathrm{H}}(H) = -\int_0^H \mathrm{d}z\, \rho(z)\left[\frac{\partial V_{\mathrm{ext}}(z, H)}{\partial z}\right] \qquad (8)$$

In eq 8, P_{H} is the pressure on the pore walls due to the confined fluid, $\rho(z)$ is the adsorbate density profile across the pore, and V_{ext} is the external pore-adsorbate potential, given by

$$V_{\mathrm{ext}}(z, H) = u_{\mathrm{sf}}(z) + u_{\mathrm{sf}}(H - z) \qquad (9)$$

where u_{sf} is the wall−fluid interaction potential. In what follows, the solvation pressure was computed as the difference between the pressure at H and the average pressure computed at wall-to-wall separations between 2.5 and 3.0 nm.

The number of adsorbed water molecules and the oxygen-atom density profile across the pore are obtained from the simulations previously discussed. Thus, it is straightforward to apply eqs 8 and 9 to our results and compute the solvation pressure by assuming that u_{sf} is equal to the Steele potential (eq 4). Simulation results at pressures close to bulk-liquid saturation were considered.

The results obtained for the solvation pressure between two infinite hydrophobic walls immersed in saturated liquid water at 298 K are given in Figure 13. In qualitative agreement with the available experimental data for the force between hydrophobic surfaces in water,[36,37] the force is long-ranged and oscillates as a function of the wall-to-wall separation. In agreement with Bratko et al.,[17] we found repulsive solvation forces at short distances

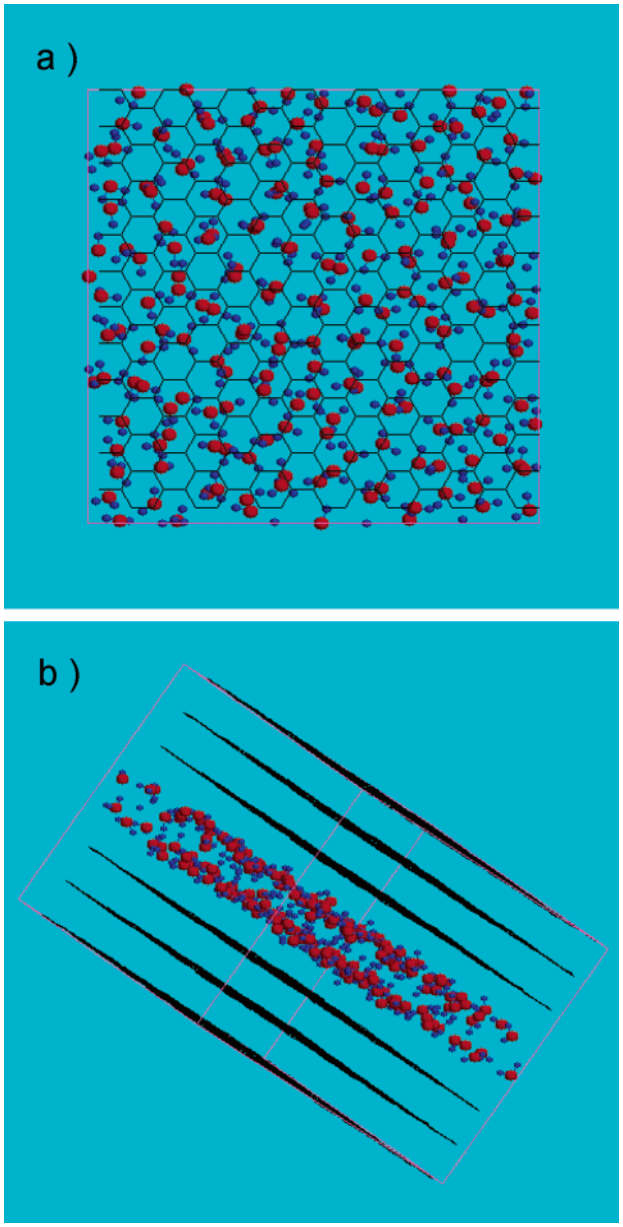

Figure 12. Top (along the z direction, part a) and lateral (along the y direction, part b) views of a typical configurational snapshot of SPC/E model water adsorbed in pores 1.0-nm wide at 298 K after pore filling. The red dots represent oxygen atoms; the blue dots represent hydrogen atoms.

($H < \sim 0.7$ nm), followed by a slight attraction at slightly larger separations ($\sim 0.7 < H < \sim 0.8$ nm). At very short separations, cavitation of metastable water confined between hydrophobic walls would generate a significant attraction between the approaching walls.[38,17] The wall-to-wall separation at which cavitation occurs depends on the details of the pore−water interactions, as well as on the external pressure, and ranges from a few nanometers for purely repulsive walls[38] to a few percents of a nanometer, as was found in this work. Qualitative agreement is found also between our results and those from Ulberg and Gubbins[9] and the recent calculations by Koga[18] for TIP4P water between hydrophobic walls. In particular, Koga found a repulsive peak at $H \sim 0.8$ nm, which is due to a bilayer-to-monolayer transition for the confined water at 270 K. Our results show repulsive

(35) Balbuena, P. B.; Berry, D.; Gubbins, K. E. *J. Phys. Chem.* **1993**, *97*, 937.
(36) Ederth, T.; Liedberg, B. *Langmuir* **2000**, *16*, 2177.
(37) Ohnishi, S.; Yaminsky, V. V.; Christenson, H. K. *Langmuir* **2000**, *16*, 8360.
(38) Lum, K.; Chandler, D.; Weeks, J. D. *J. Phys. Chem. B* **1999**, *103*, 4570.

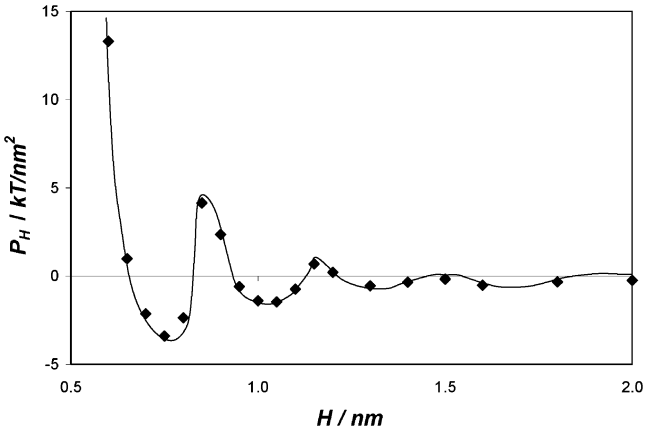

Figure 13. Solvation pressure, P_H, as a function of the wall-to-wall separation, H, for hydrophobic planes immersed in liquid water at 298 K. The line is a guide to the eye. Pore−water interactions are accounted for using the Steele potential in all the results presented here.

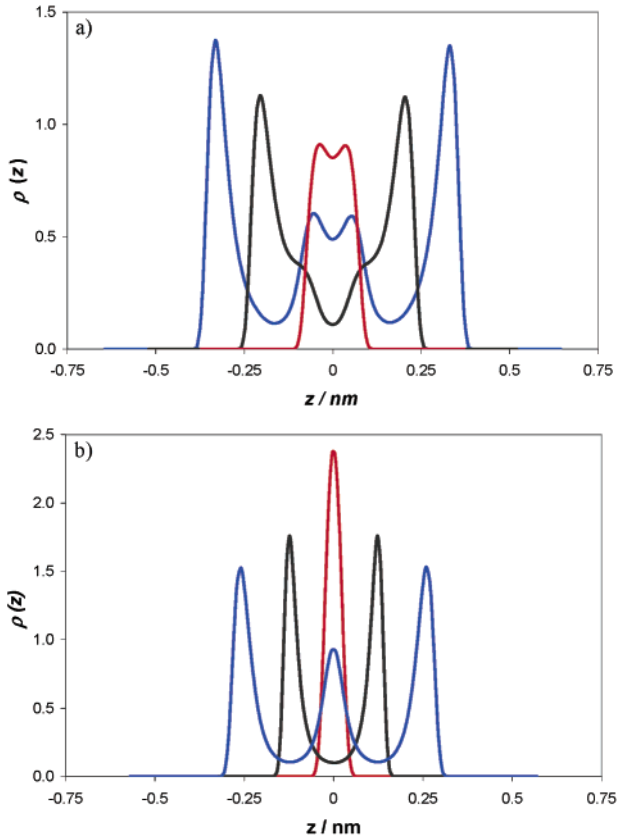

Figure 14. Representative oxygen-atom density profiles across the pore for adsorbed SCP/E water at pressures close to saturation at 298 K. Part a is for water adsorbed in pores of width 1.30 (blue line), 1.05 (black line), and 0.75 (red line) nm. Part b is for water adsorbed in pores of width 1.15 (blue line), 0.85 (black line), and 0.65 (red line) nm. Pore−water interactions are accounted for using the Steele potential in all the results presented here.

peaks at $H \sim 1.15$, 0.85, and 0.65 nm, corresponding to trilayer-to-bilayer, bilayer-to-monolayer, and monolayer-to-vapor transitions for confined water. It is interesting to note that repulsive and attractive peaks for the force profile are related to the structure of confined water. The oxygen-atom density profiles across the pore are shown in Figure 14 and correspond to attractive (Figure 14a) and repulsive (Figure 14b) peaks of the force profile. Attractive peaks correspond to separations at which confined water molecules are not allowed to form an integer number of layers between the confining walls, while repulsive peaks correspond to separations at which a finite number of layers are formed by the adsorbed water molecules; such layers are stabilized by intralayer hydrogen bonds (see Figure 11).

Summary

GCMC simulations were used to study the adsorption and desorption of SPC/E water in carbon-slit pores at 298 K. Adsorption isotherms were computed for pore widths of 0.6, 0.625, 0.7, 0.8, 1.0, 1.6, and 2.0 nm. For all pores considered, our results indicate that pore filling occurs by a capillary-condensation-like mechanism and adsorption isotherms are always characterized by adsorption/desorption hysteresis.

For pore widths narrower than 2.0 nm but larger than 0.7 nm, pore filling occurs at pressures lower than the saturation pressure for bulk water at 298 K. As a result of the more attractive pore−water interactions, the relative pressure at which pore filling occurs decreases with decreasing pore width. Moreover, the width of the hysteresis loop decreases with decreasing pore width. Water adsorption isotherms in 0.6-nm-wide pores show capillary-evaporation phenomena. This result is caused by the distortion of the hydrogen-bonded network due to the confinement of SPC/E water in such narrow pores.

Our results indicate that water is adsorbed within graphitic nanopores, and because of large adsorption−desorption hysteresis, loops may accumulate at pore constrictions, thus blocking substantial pore volume to other fluids. Because the size of the hysteresis loops decreases as the pore width decreases, carbon materials should be designed with narrower and less polydisperse pore size distributions to achieve the desired fluid separation or gas storage.

Intermediate configurational snapshots collected during the pore-filling (not shown) and pore-emptying stages of the adsorption isotherms indicate that pore filling occurs by growth of clusters of hydrogen-bonded water molecules. By contrast, pore emptying occurs with the appearance of several low-density regions (bubbles) within the confined system. Thus, the interfacial surface area is larger during pore emptying than that during pore filling.

Mean-field theory was used to compute the solvation force as a function of the wall-to-wall separation. The solvation force exhibits an oscillatory behavior as a function of the separation. Attractive peaks correspond to separations at which confined water molecules cannot establish a finite number of layers between the confining walls, whereas repulsive peaks correspond to separations at which there are a finite number of layers, stabilized by hydrogen bonding between water molecules in neighboring layers.

Acknowledgment. This work was partially supported by the LDRD Program of Oak Ridge National Laboratory (ORNL), managed by UT-Battelle, LLC, for the U.S. Department of Energy under Contract No. DE-AC05-00OR22725, and by the U.S. Department of Energy for funding under DE-FG02-98ER14847. The authors acknowledge generous allocations of computing time by NPACI, San Diego, and ORNL. A.S. thanks D. R. Cole and M. S. Gruszkiewicz (ORNL), F. R. Siperstein, C. H. Turner, J. K. Brennan, and J. P. Pikunic (NCSU) for helpful discussions, and C. M. Colina and R. Wimberly for support and encouragement.

LA0347354